Modeling of Negative Ion Production in Hydrogen Plasmas

Osamu Fukumasa

Abstract—**Effects of cesium vapor injection on H^- production in a tandem volume source are studied numerically as a function of plasma parameters. Model calculation is performed by solving a set of particle balance equations for steady-state hydrogen discharge plasmas. Here, the results with a focus on electron temperature and gas pressure dependence on H^- volume production are presented and discussed. Considering H^- surface production due to H atoms and positive hydrogen ions, enhancement of H^- production and pressure dependence of H^- production observed experimentally are qualitatively well reproduced in the model calculation, where stripping loss in the extraction and acceleration regions is taken into account. For enhancement of H^- production, so-called electron cooling in the source region, as well as in the extraction region, is not so effective if plasma parameters are initially optimized with the use of a magnetic filter.**

Index Terms—**Cesium (Cs) effect, electron cooling, H^- volume production, modeling of negative ion source, surface production.**

I. Introduction

SOURCES of H^- and D^- ions are required for generation of efficient neutral beams with energies in excess of 150 keV. The magnetically filtered multicusp ion source has been shown to be a promising source of high-quality multiampere H^- ions. In pure hydrogen discharge plasmas, most of the H^- ions are produced by the two-step process [1]–[3] which involves dissociative attachment of slow plasma electrons, e (with electron temperature, $T_e \sim 1$ eV), to highly vibrationally excited hydrogen molecules, $H_2(v'')$. Recent experimental investigations have revealed that the addition of cesium (Cs) or barium to a hydrogen discharge can enhance the H^- output current by a several factor and cause a substantial reduction in the electron-to-H^- ratio in the extracted beam [4], [5]. It has also been reported [6], [7] that the optimum pressure $p_{\rm opt}$ giving the highest H^- current for a certain arc current I_a is almost independent of I_a and that the value of $p_{\rm opt}$ decreases to 0.8–1.0 Pa when Cs vapor is seeded into a plasma source. Although these effects have been observed by many researchers, the mechanism of Cs catalysis in H^- production remains to be clarified.

To date, we have studied source modeling [2], [3], [8] and Cs effects on enhancement of H^- yield [9]–[11]. The mechanisms underlying Cs injection enhancement of H^- production are reported to be as follows [4]:

1) electron cooling;
2) production of $H_2(v'')$ due to reaction between Cs atoms and H_3^+;
3) H^- surface production caused by H atoms and positive hydrogen ions.

Based on some experimental results (for example, correlation between the H^- current and the work function of the plasma grid [12] and dependence of H^- current on barium washer voltage [13]), we assume that the dominant process of enhancement is surface production, where the surface has a low work function because of the Cs coverage. In this paper, to elucidate further the Cs effects, we will discuss enhancement of H^- yield as functions of some plasma parameters, i.e., electron density n_e, hydrogen gas pressure p and T_e [14]. Taking into account H^- surface production, the model calculation well reproduces the characteristic features of enhancement of H^- production observed experimentally [6], [7].

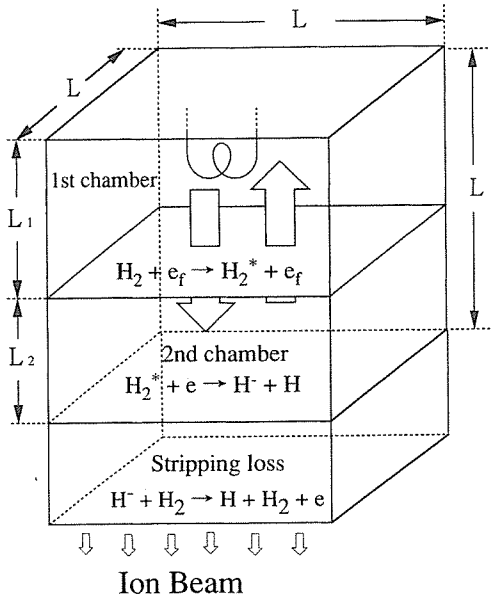

Fig. 1. Simulation model for the tandem two-chamber system.

II. Simulation Model

To study H^- production in a tandem two chamber system, we used the simulation model [2], [3], [8] shown in Fig. 1. Two chambers of volume $L \times L \times L_1$ (the first) and $L \times L \times L_2$ (the second) are in contact with each other in the region of magnetic filter, where $L = L_1 + L_2 = 30$ cm. We assume that fast electrons, e_f, are present only in the first chamber because the magnetic filter prevents e_f from entering the second chamber.

Manuscript received December 14, 1998; revised March 22, 2000. This work was supported by a Grant-in-Aid for Scientific Research from the Japanese Ministry of Education, Science, Sports and Culture.

The author is with the Department of Electrical and Electronic Engineering, Yamaguchi University, Ube 755-8611, Japan.

Publisher Item Identifier S 0093-3813(00)05708-8.

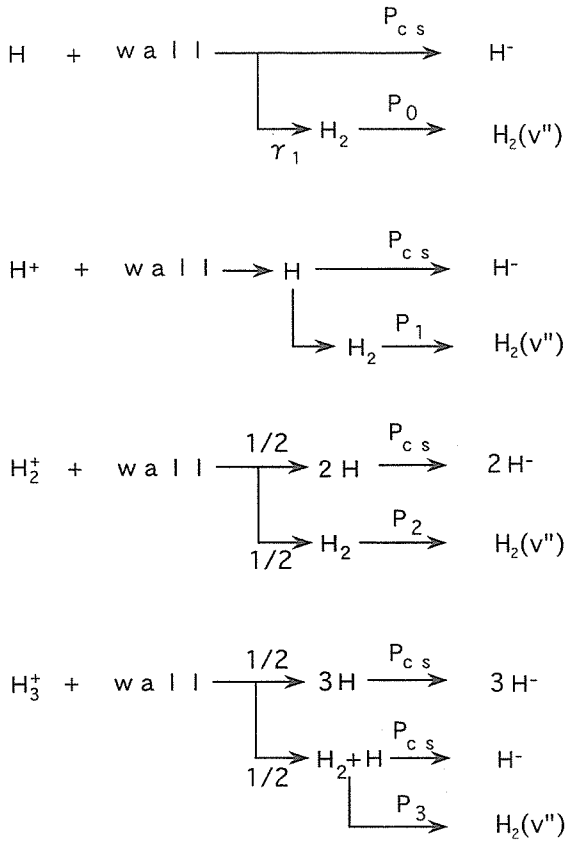

Fig. 2. Reaction processes at the wall surface considered in the present modeling.

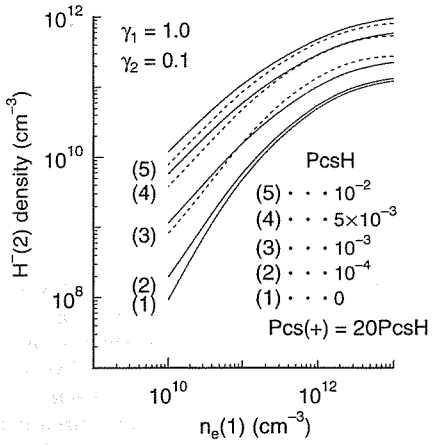

Fig. 3. Effects of the surface production due to both H atoms and positive ions on enhancement of H^- production : H^- density, $H^-(2)$, in the second chamber versus electron density, $n_e(1)$, in the first chamber. Solid lines and dashed lines are corresponding to the case of electron temperature in the first chamber $T_e(1) = 5$ eV, and $T_e(1) = 3$ eV, respectively. Other numerical conditions are as follows: Hydrogen gas pressure $p(H_2) = 0.67$ Pa (5 mtorr), electron temperature in the second chamber $T_e(2) = 1$ eV, $\gamma_1 = 1.0$, and wall parameter γ_2 for $H_2(v'')$ is 0.1. Parameter is the probability of H^- formation from H at the wall, P_{csH}.

We consider four ion species (H^-, H^+, H_2^+, and H_3^+), two electron species (e and e_f) and three species of neutral particles [H, $H_2(v'')$, and H_2]. We assume that the ion containment time ratio $\tau(H^+) : \tau(H_2^+) : \tau(H_3^+) = 1 : \sqrt{2} : \sqrt{3}$, and we treat $\tau(H^+)$ as one of the unknown independent variables. Particles other than e and e_f are assumed to move freely between the two chambers without being influenced by the filter. Here we assume that ions move freely across the magnetic filter. Because, the strength of the magnetic filter is usually selected to influence only electron dynamics. The number of particles passing through the filter is represented by flux nv, where n and v are the particle density and velocity, respectively.

In the present model, two kinds of reaction process at the wall surface are included. One is H^- surface production caused by Cs injection. The following four processes are considered [9]–[11], [14], [15]: $H_n^+ + \text{wall} \rightarrow nH^-(n = 1, 2, 3)$, and $H + \text{wall} \rightarrow H^-$. The other is effect of $H_2(v'')$ surface production due to wall recombination of H and neutralization of positive ions [16], [17]. Wall effects considered in the present study are summarized in Fig. 2.

In modeling, surface production rates of negative ions are estimated as follows: The term representing wall loss of H atoms is expressed as $-(\gamma_1 + P_{csH})N_H/\tau_H$, where γ_1 is a wall recombination coefficient, P_{csH} indicates the probability of H^- formation at the wall, N_H is H density, and τ_H is a confinement time of H. Then, the H^- production rate at the wall surface is expressed as $P_{csH}N_H/\tau_H$. We also assume that recombination of H to H_2 at the wall is written as $\gamma_1 N_H/(2\tau_H)$. Therefore, production of $H_2(v'')$ is expressed as $P_0\gamma_1 N_H/(2\tau_H)$, where P_0 is the probability of finding $H_2(v'')$ in H_2 formed at the wall. In the same way, the rates of production of H^- and $H_2(v'')$ from positive ions at the wall are also estimated.

For each chamber, 19 rate equations for H, $H_2(v'' = 1$–$14)$, H^-, H^+, H_2^+, and H_3^+ are derived by taking into account the above mentioned reaction processes, other collisional reaction processes occurring in hydrogen plasma [2] and the interaction between the two chambers. Besides these rate equations, there are two constraints for each chamber: i.e., the charge neutrality and particle number conservation. Thus, for the tandem two-chamber system, a set of 42 equations is solved numerically as a function of plasma parameters.

III. Numerical Results and Discussion

The procedure for numerical simulation is as follows: To determine the electron density dependence of the H^- production, calculations are performed for various electron densities, $n_e(1)$, in the first chamber on the assumption that other plasma parameters are kept constant: i.e., for example, the electron density ratio between two chambers $n_e(2)/n_e(1) = 0.2$, density of e_f in the first chamber $n_{fe}(1)/n_e(1) = 0.05$, $p = 0.67$ Pa(5 mtorr), T_e in the first chamber $T_e(1) = 5$ eV and T_e in the second chamber $T_e(2) = 1$ eV, and the filter position $L_1 : L_2 = 28 : 2$ cm. According to previously obtained results [2], [3], these plasma conditions were chosen to be reasonable in the typical negative ion sources and to nearly optimize H^- pure-volume production in the second chamber. Those plasma conditions are also used in the present study.

Fig. 3 shows the H^- densities, $H^-(2)$, in the second chambers for various different values of P_{cs}. Wall conditions are as follows. For positive ions, $P_{cs1} = P_{cs2} = P_{cs3} = P_{cs}(+)$, and $P_{cs}(+) = 20P_{csH}$. $P_0 = P_1 = 0.01$, and $P_2 = P_3 = 0.3$. When $P_{csH} = 0$, i.e., curve (1), H^- ions are produced by the so-called two-step pure volume process. With in-

creasing P_{csH}, as was shown previously [9]–[11], [14], $H^-(2)$ increases markedly. In a high-density region, i.e., at $n_e(1) = 5 \times 10^{12}$ cm^3, $H^-(2)$ is enhanced by a factor of four for curve (4) and by a factor of seven for curve (5). Since the same factor of enhancement was obtained when the effect of surface H^- production in only the second chamber was taken into account, one can conclude that the second chamber is the most effective area for surface enhancement of H^- production. In the present simulation, as the magnetic filter is set at $L_1 = 28$ cm, the total area of the wall surface in the second chamber is nearly equal to the area of the end wall, which corresponds to the plasma grid of the tandem volume sources [6], [7]. Thus, the numerical results above mentioned agree well qualitatively with the experimental results [6], [7], [12], [13]. As determined experimentally, the H^- yield rises with plasma grid temperature peaking at around 250 °C [6] or 300 °C [7] . This spatial or localized dependence of H^- production enhancement is caused not by a volume process but by a surface process.

Electron cooling comes from the Cs-ionization energy loss of the electrons, and the ionization may occurs mainly in the first chamber. Therefore, cooling effect appears as the lowering of the electron temperature $T_e(1)$ in the first chamber. For reference, in Fig. 3, we also plot the numerical results $H^-(2)$ obtained under $T_e(1) = 3$ eV, namely the three dashed lines corresponding to the same P_{csH} for curves (3), (4), and (5). Although details are discussed in the later paragraph, electron cooling does not affect strongly $H^-(2)$ density.

Theoretically, the probability β^- of incoming H atoms being converted to H^- ions on the wall is given as $\beta^- = (2/\pi)\exp[-\pi(\phi - A)/2a\nu]$ [18], where ϕ is the work function, A is the electron affinity, a is the decay constant, and ν is the normal velocity of the incident particle. The effect of Cs is expressed through the value of ϕ. For example, ϕ is 1.45 eV for the surface covered with half of a monolayer of Cs and 2.1 eV for the surface covered with a monolayer of Cs. If we take the temperature of H atoms to be 0.5 eV,$\phi = 1.8$ eV [12] and $a = 3.08 \times 10^{-5}$ eV · s/m [18], [19], we can estimate $\beta^- = 4.87 \times 10^{-3}$ for H atoms. Impinging positive ions will be accelerated by sheath potential. Namely, positive ions have rather large ν compared with H. For protons with energy of 1 eV, β^- is 2.05×10^{-2}. Therefore, the probability of incoming positive ions being converted to H^- ions on the wall could be much higher than that of thermal H atoms [20]. Then, in the present calculation, $P_{cs}(+) = 20P_{csH}$. Although P_{csH} is treated as a numerical parameter, values of P_{csH} are quite reasonable except that $P_{csH} = 10^{-2}$. To discuss Cs effects quantitatively, we must estimate precisely the relationship between P_{cs} in our simulation and the theoretical value β^- for the corresponding experiment.

As described above, electron cooling comes from the Cs-ionization energy loss of the electrons. The ionization occurs mainly in the first chamber. Therefore, cooling effect appears as the lowering of the electron temperature $T_e(1)$ in the first chamber and the cooling of $T_e(2)$ in the second chamber may be only a result of cooling of $T_e(1)$. In the present study, for discussion of the effect of electron cooling due to Cs injection, model calculation has been performed as a function of both

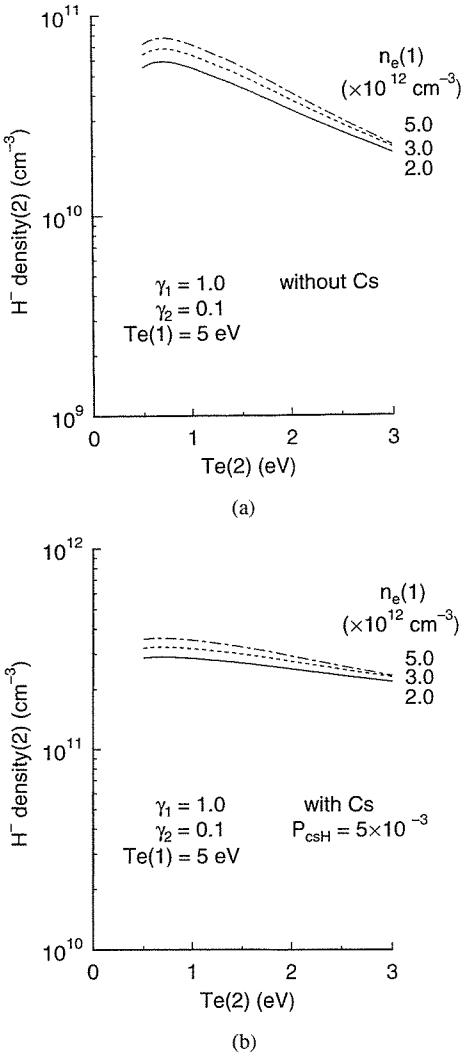

Fig. 4. Dependence of H^- production on electron temperature: $H^-(2)$ versus $T_e(2)$ in the second chamber: (a) without Cs and (b) with Cs, where $p(H_2) = 0.67$ Pa and $T_e(1) = 5$ eV. Parameter is $n_e(1)$.

$T_e(1)$ and $T_e(2)$, respectively. Here, wall condition is described by curve (4) in Fig. 3, and the parameter is $n_e(1)$.

Fig. 4 shows $T_e(2)$ dependence of H^- production without and with Cs. Production rates and destruction probabilities corresponding to the results in Fig. 4 are shown in Figs. 5 and 6. For the pure-volume case, as is shown in Fig. 4(a), $H^-(2)$ depends strongly on $T_e(2)$. This is explained as follows: The predominant production process is dissociative attachment, i.e., $H_2(v'') + e \rightarrow H^- + H$, VP in Fig. 5(a). Its reaction rate has a maximum value at $T_e = 0.5$–1.0 eV and then decreases with T_e. For destruction of H^- ions, according to the result in Fig. 5(b), electron detachment caused by e, i.e., $H^- + e \rightarrow H + 2e$, increases abruptly with T_e and its reaction rate is predominant ($T_e \geq 2$ eV). Then, with decreasing $T_e(2)$, $H^-(2)$ increases and then reaches the maximum value at about 0.7 eV [2]. In real ion sources, usually, $T_e(2)$ is well optimized, i.e., $T_e \simeq 1$ eV, with the use of magnetic filter. On the other hand, in the presence of Cs as shown in Fig. 4(b), $H^-(2)$ hardly depends on $T_e(2)$, especially in the region of 1 eV, compared with the results in the pure-volume case. Because, the enhancement of H^- production due to surface processes is so marked that the increase in H^-

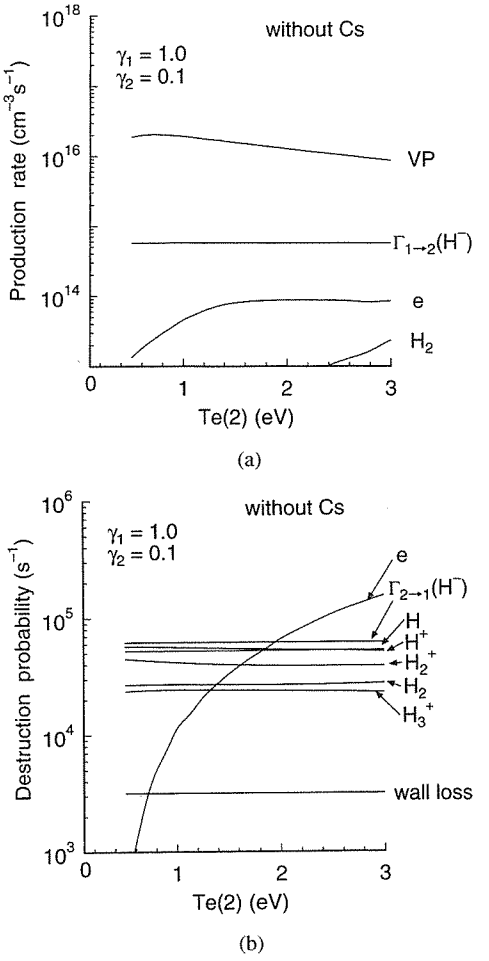

Fig. 5. (a) Production rates and (b) destruction probabilities versus $T_e(2)$, corresponding to the $H^-(2)$ density without Cs shown in Fig. 4(a), where $n_e(1) = 5 \times 10^{12}$ cm^{-3} and $T_e(1) = 5$ eV.

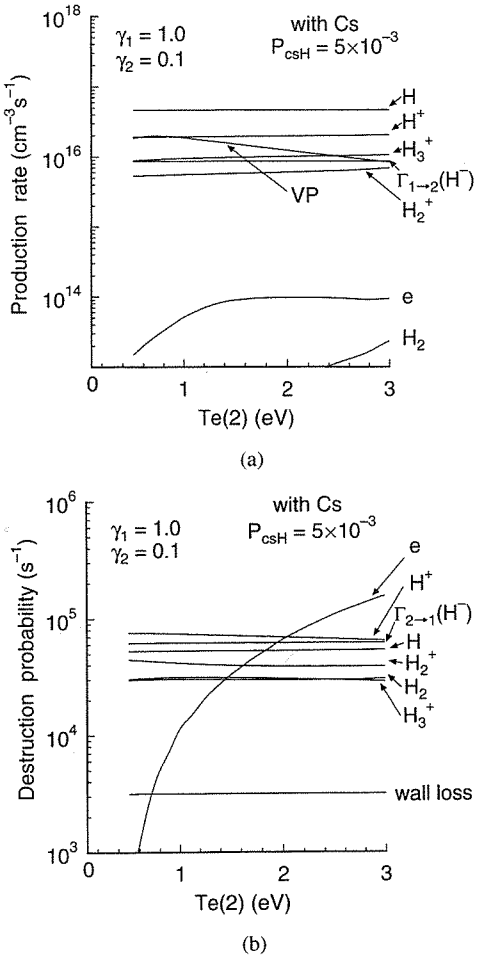

Fig. 6. (a) Production rates and (b) destruction probabilities versus $T_e(2)$, corresponding to the $H^-(2)$ density with Cs shown in Fig. 4(b), where $n_e(1) = 5 \times 10^{12}$ cm^{-3} and $T_e(1) = 5$ eV.

density due to a small reduction of T_e could be masked. For destruction of H^- ions, however, collisional processes are nearly the same as ones in the pure-volume case (see Fig. 6). With increasing T_e, electron detachment caused by e becomes predominant, and then H^- density gradually decreases with T_e.

Fig. 7 shows $T_e(1)$ dependence of H^- production in the presence of Cs. The enhancement of H^- production due to surface production processes is so marked, and $H^-(2)$ keeps nearly constant for the change of $T_e(1)$. Strictly speaking, $H^-(2)$ decreases gradually with decreasing $T_e(1)$. Because, with decreasing $T_e(1)$, surface production of H^- caused by H and H^+ decreases.

In the present parametric study, surface production rates are treated as numerical parameters and are kept constant corresponding to the variation of T_e. In general, for example, with varying $T_e(2)$, potential difference between plasma and chamber wall may change and it changes the value of P_{cs}. However, in the real ion source, surface production of H^- ions mainly occur at the surface of the plasma grid [6], [7]. As described in discussion of Fig. 3, we also reconfirm this point by the present model calculation. Beside these, in experiment, potential difference between the plasma grid and plasma is varied easily by changing grid bias voltage [13], [21], and potential difference can be kept optimum value for

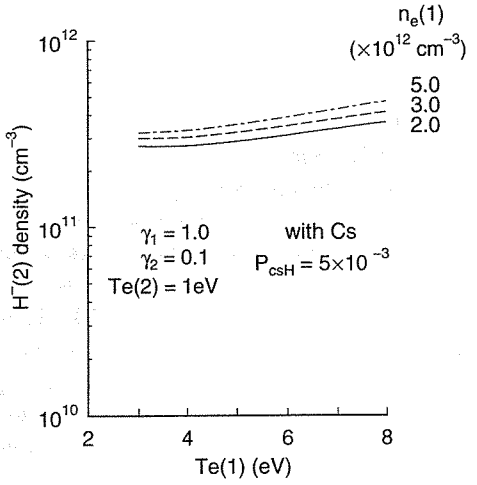

Fig. 7. Dependence of H^- production on electron temperature: $H^-(2)$ with Cs versus $T_e(1)$ in the first chamber, where $p(H_2) = 0.67$ Pa and $T_e(2) = 1$ eV. Parameter is $n_e(1)$.

surface production with different plasma conditions. In this case, calculation with constant P_{cs} is more suitable for the experimental conditions. Then, to obtain the general feature of $T_e(2)$ dependence, in the present calculation, we do calculation by using constant P_{cs}.

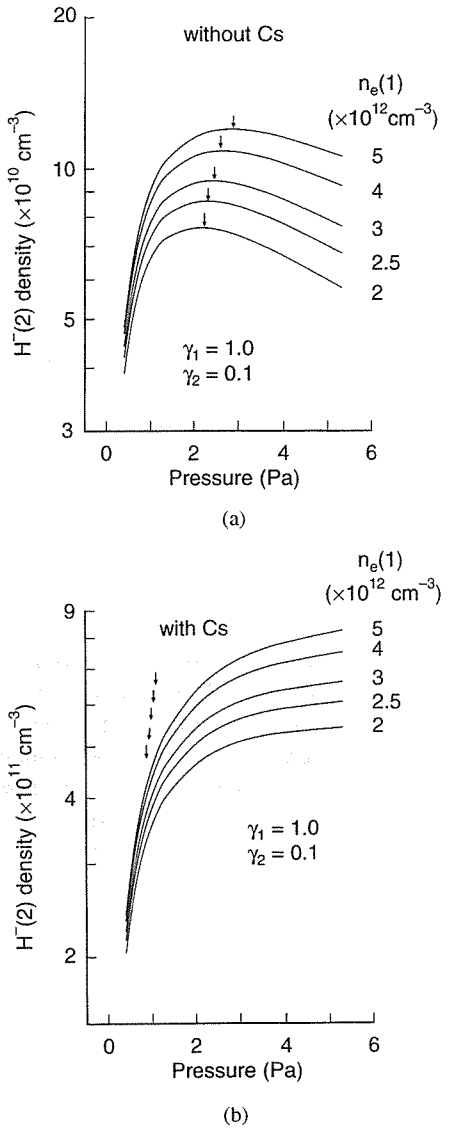

Fig. 8. Effects of hydrogen gas pressure on H^- production: $H^-(2)$ versus gas pressure p: (a) without Cs and (b) with Cs. In (a), the arrows show the point where H^- density is maximum. In (b), the arrows show the point where H^- density corresponds to four times the maximum H^- density in the absence of Cs where $T_e(1) = 5$ eV and $T_e(2) = 1$ eV. Parameter is $n_e(1)$.

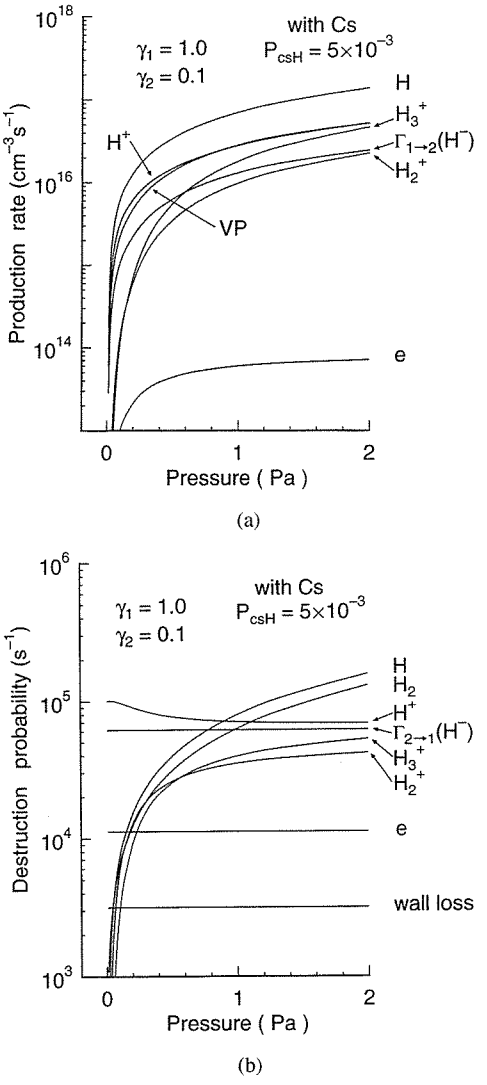

Fig. 9. (a) Production rates and (b) destruction probabilities versus p, corresponding to the $H^-(2)$ density shown in Fig. 8(b) where $n_e(1) = 5 \times 10^{12}$ cm^{-3}.

As a whole, T_e dependence of $H^-(2)$ keeps the same tendency as shown in Figs. 4 and 7 although enhancement of $H^-(2)$ varies with the change of surface production rates. Namely, according to the results shown in Figs. 4 and 7, effect of electron cooling due to Cs injection is as follows: $H^-(2)$ decreases gradually with decreasing $T_e(1)$ (see Fig. 7) and $H^-(2)$ hardly depends on $T_e(2)$ in the region of 1 eV [see Fig. 4(b)]. Therefore, electron cooling is not so effective for enhancing H^- yield, if plasma parameters including T_e are well optimized before Cs injection with the use of the magnetic filter and the plasma grid. In experiment, however, electron cooling seems to be one of the reasons for the reduction in the electron-to-H^- ratio in the extracted beam.

Next, we will discuss pressure dependence of H^- production or of the extracted H^- current. Fig. 8 shows $H^-(2)$ as a function of p for various $n_e(1)$. In this calculation, the wall conditions are described by curve (4) in Fig. 3. In Fig. 8(a), i.e., in the absence of Cs, H^- ions are produced by a pure-volume process. Apparently, there is an optimum pressure $p_{\rm opt}$ for each $n_e(1)$, and the value of $p_{\rm opt}$ increases with $n_e(1)$ (see the arrows in the figure). On the other hand, in Fig. 8(b), i.e., in the presence of Cs, the pressure dependence of $H^-(2)$ for each $n_e(1)$ has almost the same pattern. As in the low-pressure region, enhancement of H^- production also appears clearly, the arrows which show the points where $H^-(2)$ corresponds to four times the value for $H^-(2)$ in the pure volume case shift to the low-pressure region. In this case, however, no optimum pressures are observed clearly.

Fig. 9 shows the production rate and destruction probability of $H^-(2)$ corresponding to the result in Fig. 8(b), where $n_e = 5 \times 10^{12}$ cm^{-3}. The predominant production process is surface production due to H. At $p = 1$ Pa, for example, both surface production due to H^+ and volume production VP have next dominant contribution, and the contribution of H_3^+ is the third. At $p = 1$ Pa, the density distribution of $H^+ : H_2^+ : H_3^+$ in the second chamber is 49 : 24 : 27. Probability of H^- surface production from H_3^+ is effectively twofold larger than that from H_2^+.

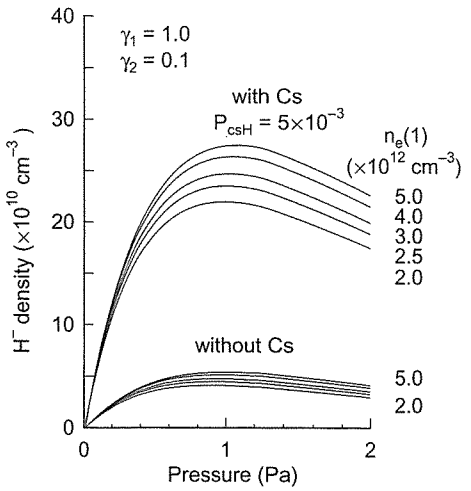

Fig. 10. Pressure dependence of the extracted H^- ions: H^- density versus p, corresponding to the results shown in Fig. 8, where stripping loss of H^- ions in the extraction and acceleration grids region is included.

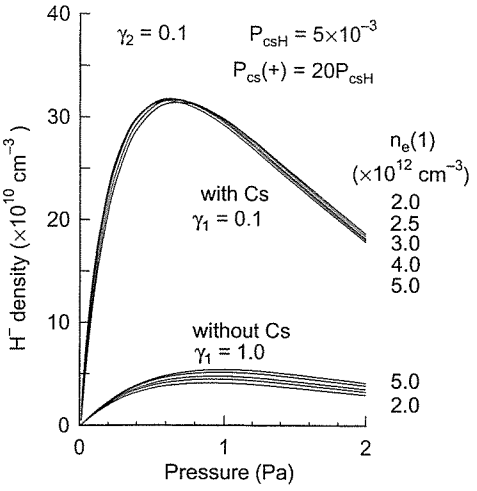

Fig. 11. Pressure dependence of the extracted H^- ions: H^- density versus p. In this simulation, wall parameter γ_1 is varied from 1.0 (without Cs) to 0.1 (with Cs). Parameter is $n_e(1)$.

For destruction of H^- ions, electron detachments caused by H and H_2 are predominant when $p > 1$ Pa. In the low-pressure region ($p \leqq 1$ Pa), however, both electron detachments caused by H^+ and loss flux of negative ions $\Gamma_{2\to1}$, i.e., flow of $H^-(2)$ across the filter to the first chamber, are predominant.

Usually, experimental results, except those in [22], show the extracted H^- current as a function of p. In [6] and [7], the H^- current is enhanced severalfold, and $p_{\rm opt}$ is reduced to 0.5–0.8 Pa and is almost constant irrespective of I_a or arc power $P_{\rm arc}$. As described in [22], $p_{\rm opt}$ is reduced again to 0.3–0.4 Pa, although $p_{\rm opt}$ increases gradually with $P_{\rm arc}$. Fig. 8, however, shows not the extracted H^- current but the H^- density in the second chamber. Therefore, strictly speaking, we could not directly compare the numerical results shown in Fig. 8 with the experimental ones. Because, the pressure dependence of H^- current depends strongly on stripping loss of H^- ions along the beam axis [7], [23], [24].

In order to discuss pressure dependence of the extracted H^- current, we derive the extracted H^- ions from $H^-(2)$ by taking into account stripping loss of H^- ions in the extraction and acceleration grids region (see Fig. 1). According to gas pressure distribution along the beam axis estimated by the Monte Carlo simulation [24], we calculate the survival factor F against the stripping loss of H^- ions, i.e., $H^- + H_2 \to H + H_2 + e$ and $H^- + H \to 2H + e$. F is a decreasing function of pressure.

Fig. 10 shows the extracted H^- ions, corresponding to the results in Fig. 8, as a function of p. They are the product of $H^-(2)$ in Fig. 8 with F. In the absence of Cs, $p_{\rm opt}$ is observed again for each $n_e(1)$, and the value of $p_{\rm opt}$ increases with $n_e(1)$. In experiment [6], [22], this is a typical tendency in a multicusp volume source where the parameter is not n_e, but arc current I_a. With Cs injection, H^- density increases by several times. Furthermore, in the present case, $p_{\rm opt}$ also appears clearly. This comes from the pressure dependence of F. Namely, F decreases sharply with pressure. However, $p_{\rm opt}$ does not shift to low-pressure region as observed in some experiments [6], [7].

Fig. 11 shows another example of pressure dependence of the extracted H^- ions [25]. In this case, the value of γ_1 with Cs is reduced to 0.1 and then $p_{\rm opt}$ shifts to lower-pressure region compared with the results without Cs. This tendency agrees with experiments. As γ_1 is a parameter for controlling H density, this suggests that H density plays an important role in H^- production with Cs. H density increases with decreasing γ_1. Therefore, we speculate that H density in hydrogen discharge with Cs becomes higher compared with that in pure hydrogen discharge. Details are now under study.

Recently, modeling of negative ion transport in a plasma source was reported [26]. This code can be used to calculate the extraction probability of negative ions produced at any location inside the source. In the future, we will discuss the extraction of negative ions with the use of our model calculation and the idea of the above mentioned code.

IV. Conclusion

We have theoretically studied Cs effects on enhancement of H^- yield and plasma parameter dependence of H^- density in negative-ion volume sources. Considering H^- surface production, enhancement of H^- production and pressure dependence of H^- production observed experimentally are qualitatively well reproduced in the model calculation, where stripping losses in the extraction and acceleration regions are taken into account. H^- surface production due to H and positive ions (H^+ and H_3^+) contribute predominantly to H^- enhancement. For destruction of H^-, H, and H_2 contribute predominantly. Detailed discussion including another wall effect of γ_1 will be reported in a forthcoming paper. For enhancement of H^- production, electron cooling (due to cesium ionization energy loss of electrons) is not so effective if plasma parameters in the absence of cesium are well optimized with magnetic filter.

Acknowledgment

The author would like to thank E. Niitani, K. Yoshino, and H. Monji for their assistance in numerical calculations.

REFERENCES

[1] J. R. Hiskes and A. M. Karo, "Generation of negative ions in tandem high-density hydrogen discharges," *J. Appl. Phys.*, vol. 56, pp. 1927–1938, 1984.

[2] O. Fukumasa, "Numerical studies on the optimization of volume-produced H^- ions in the single-chamber system," *J. Phys. D*, vol. 22, pp. 1668–1679, 1989.

[3] O. Fukumasa and S. Ohashi, "Numerical study on tandem source for production of negative ions," *J. Phys. D*, vol. 22, pp. 1931–1934, 1989.

[4] S. R. Walther, K. N. Leung, and W. B. Kunkel, "Production of H^- ions with addition of cesium or xenon to a hydrogen discharge in a small multicusp ion source," *J. Appl. Phys.*, vol. 64, pp. 3424–3428, 1988.

[5] K. N. Leung, C. A. Hauck, W. B. Kunkel, and S. R. Walther, "Optimization of H^- production from a small multicusp ion source," *Rev. Sci. Instrum.*, vol. 60, pp. 531–538, 1989.

[6] Y. Okumura, N. Hanada, T. Inoue, H. Kojima, Y. Matsuda, Y. Ohara, M. Seki, and K. Watanabe, "Cesium mixing in the multi-ampere volume H^- ion source," in *Proc. 5th Int. Symp. Production Neutralization Negative Ions Beams*, New York, 1990, pp. 169–183.

[7] A. Ando, T. Tsumori, Y. Oka, O. Kaneko, Y. Takeiri, E. Asano, T. Kawamoto, R. Akiyama, and T. Kuroda, "Large current negative hydrogen ion beam production," *Phys. Plasmas 1*, pp. 2813–2815, 1994.

[8] O. Fukumasa, "Effects of the energy distribution of fast electrons on H_2 vibrational excitation in a tandem negative ion source," *J. Appl. Phys.*, vol. 71, pp. 3193–3196, 1992.

[9] O. Fukumasa, H. Naitou, and T. Tanebe, "Modeling effects of cesium vapor injection in a volume H^- ion source," in *Proc. 6th Int. Symp. Production Neutralization Negative Ions Beams*, New York, 1992, pp. 117–129.

[10] O. Fukumasa, T. Tanebe, and H. Naitou, "Identification of cesium effects on enhancement of H^- production in a volume negative ion source," *Rev. Sci. Instrum.*, vol. 65, pp. 1213–1215, 1994.

[11] O. Fukumasa and E. Niitani, "Numerical study of cesium effects on negative ion production in volume sources," in *Proc. 7th Int. Symp. Production Neutralization Negative Ions Beams*, New York, 1995, pp. 187–197.

[12] Y. Okumura, Y. Fujiwara, T. Inoue, K. Miyamoto, N. Miyamoto, A. Nagase, Y. Ohara, and K. Watanabe, "High power negative ion sources for fusion at the Japan Atomic Energy Reseach Institute," *Rev. Sci. Instrum.*, vol. 67, pp. 1092–1097, 1996.

[13] K. N. Leung, C. F. A. van Os, and W. B. Kunkel, "H^- enhancement process in a multicusp ion source operated with a barium insert structure," *Appl. Phys. Lett.*, vol. 58, pp. 1467–1469, 1991.

[14] O. Fukumasa and E. Niitani, "Pressure dependence of negative hydrogen ion production in a cesium seeded tandem volume source," *Jpn. J. Appl. Phy.*, vol. 35, pp. L1528–L1531, 1996.

[15] M. Ogasawara, K. Miyamoto, and R. Sakurai, "An estimate of surface effect in ion source," in *Proc. IAEA Tech. Comm. Mtg. Negative Ion Based Neutral Beam Injections*: JAERI, 1991, pp. 99–104.

[16] J. R. Hiskes and A. M. Karo, "Recombination and dissociation of H_2^+ and H_3^+ ions on surfaces to form $H_2(v'')$: negative-ion formation on low-work-function surface," *J. Appl. Phys.*, vol. 67, pp. 6621–6632, 1990.

[17] O. Fukumasa, K. Mutou, and H. Naitou, "Numerical study on production processes on vibrationally excited molecules in hydrogen negative ion sources," *Rev. Sci. Instrum.*, vol. 63, pp. 2693–2695, 1992.

[18] B. Rasser, J. N. M. Van Wunnik, and J. Los, "Theoretical models of the negative ionization of hydrogen on clean tungsten, cesiated tungsten and cesium surfaces at low energies," *Surf. Sci.*, vol. 118, pp. 697–710, 1982.

[19] T. Okuyama, private communication, 1992.

[20] P. Berlemont, D. A. Skinner, and M. Bacal, "Modeling surface effects in negative-ion volume sources," *Chem. Phys. Lett.*, vol. 183, pp. 397–402, 1991.

[21] T. Takanashi, Y. Takeiri, O. Kaneko, Y. Oka, K. Tsumori, and T. Kuroda, "Plasma characteristics of a large RF-driven negative hydrogen ion source," *Jpn. J. Appl. Phys.*, vol. 35, pp. 2356–2362, 1996.

[22] C. Courteille, A. M. Bruneteau, and M. Bacal, "Investigation of a large volume negative ion source," *Rev. Sci. Instrum.*, vol. 66, pp. 2533–2540, 1995.

[23] M. Ogasawara, R. Sakurai, T. Koishimine, S. Mitsuhashi, and A. Hatayama, "Numerical simulation of a hybrid negative ion source," *Fusion Eng. Design*, vol. 26, pp. 507–521, 1995.

[24] Y. Takeiri, A. Ando, O. Kaneko, Y. Oka, K. Tsumori, R. Akiyama, E. Asano, T. Kawamoto, T. Kuroda, M. Tanaka, and H. Kawakami, "Development of an intense negative hydrogen ion source with an external magnetic filter," *Rev. Sci. Instrum.*, vol. 66, pp. 2541–2546, 1995.

[25] O. Fukumasa and H. Monji, "Parametric study of negative ion production in cesium seeded hydrogen plasmas," *Rev. Sci. Instrum.*, vol. 71, pp. 1234–1236, 2000.

[26] D. Riz and J. Pamela, "Modeling of negative ion transport in a plasma source," *Rev. Sci. Instrum.*, vol. 69, pp. 914–919, 1998.

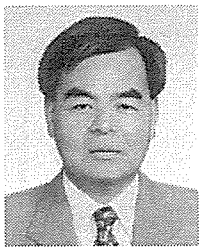

Osamu Fukumasa was born in Kobe, Japan, on January 8, 1946. He received the B.E. degree in 1968 from Nagoya Institute of Technology, Japan and the M.E. and D.E. degrees in 1970 and 1981, respectively, from Kyoto University, Japan.

From 1973 to 1981, he was with the Department of Electrical Engineering, Kyoto University. He was a Lecturer in 1982, an Associate Professor in 1983, and a Professor in 1988 at Yamaguchi University, Japan. He is presently a Professor with the Department of Electrical and Electronic Engineering, Yamaguchi University. His research field is in the development of negative ion sources for neutral beam injectors, thermal plasma material processing, and production and control of reactive plasmas.